New Journal of Physics
The open access journal at the forefront of physics

Deutsche Physikalische Gesellschaft DPG
IOP Institute of Physics

Published in partnership with: Deutsche Physikalische Gesellschaft and the Institute of Physics

OPEN ACCESS

RECEIVED
19 October 2017

REVISED
11 December 2017

ACCEPTED FOR PUBLICATION
21 December 2017

PUBLISHED
5 February 2018

PAPER

Maxwell's demon in the quantum-Zeno regime and beyond

G Engelhardt[1,2] and G Schaller[1]

[1] Institut für Theoretische Physik, Technische Universität Berlin, Hardenbergstr. 36, D-10623 Berlin, Germany
[2] Beijing Computational Science Research Center, Beijing 100193, People's Republic of China

E-mail: georg.engelhardt@csrc.ac.cn

Keywords: Maxwell's demon, quantum-Zeno effect, feedback control, electronic transport, open quantum systems

Abstract

The long-standing paradigm of Maxwell's demon is till nowadays a frequently investigated issue, which still provides interesting insights into basic physical questions. Considering a single-electron transistor, where we implement a Maxwell demon by a piecewise-constant feedback protocol, we investigate quantum implications of the Maxwell demon. To this end, we harness a dynamical coarse-graining method, which provides a convenient and accurate description of the system dynamics even for high measurement rates. In doing so, we are able to investigate the Maxwell demon in a quantum-Zeno regime leading to transport blockade. We argue that there is a measurement rate providing an optimal performance. Moreover, we find that besides building up a chemical gradient, there can be also a regime where the feedback loop additionally extracts energy, which results from the energy non-conserving character of the projective measurement.

1. Introduction

Maxwell's demon is the central character in a long-standing gedankenexperiment suggested by Maxwell in 1871, which challenges the validity of the second law of thermodynamics [1, 2]: a box containing an ensemble of particles is divided in two compartments. The Maxwell demon observes the particles and has the ability to open and close a door such that only fast particles can enter the 'left' compartment, while slow particles leave the 'left' compartment. In doing so, the demon can build up a thermal gradient, which can later be used to run a thermal engine. However, as the opening and closing does not consume energy in the ideal case, this procedure would violate the second law of thermodynamics saying that such a perpetuum mobile of the second kind is not possible. This paradox was resolved by Landauer by recognizing that the Maxwell demon has to delete information in order to perform its task. This is directly related to heat dissipation [3–6].

This article provides a quantum mechanical treatment of Maxwell's demon. In quantum mechanics the action of the Maxwell demon is more involved due to the special meaning of the observation or measurement of the particles, namely the wave-function-collapse postulate. A quantum measurement thus does not leave the system state unaffected so that the observation by the Maxwell demon necessarily affects the dynamics. Here we investigate these quantum implications at the example of a single-electron transistor (SET). We implement the Maxwell demon using a piecewise-constant feedback scheme, where the system state is observed after time periods τ and the system parameters are adjusted accordingly. This feedback scheme has been already successfully implemented in experiment [7]. For other experimental and theoretical feedback-related approaches in mesoscopic devices to extract work or to achieve similar objectives we refer to [8–27].

In this article, we harness a dynamical coarse-graining (DCG) method [28]. This method provides interesting properties which are perfectly suitable for the issues which we are interested in. The DCG is designed in a way so that it becomes exact for short evolution times in contrast to a Born–Markov master equation or other coarse-graining approaches [29–31]. For this reason, it is favorable to use it to describe the piecewise-constant feedback protocol for high measurement rates, as in this case the time-evolution is repeatedly restarted after each measurement.

In contrast to other methods as, e.g., the so-called Redfield equation, the DCG ensures complete positivity for all times [28, 32, 33], so that thermodynamic quantities, e.g., the system entropy, are guaranteed to be well defined for all time instants. Moreover, [34] shows that this technique even accounts for highly non-Markovian effects observable in the coherence or the entanglement dynamics. Furthermore, this approach can be amended for a full-counting statistics treatment in systems under non-equilibrium conditions [35].

The DCG thus provides a reliable accuracy for the parameter range which we are interested in. This article goes beyond the treatment in [13], where the time dynamics has been approximated by a Born–Markov master equation.

While investigating short feedback times, we unavoidably run into another long-standing paradox of physics, namely the quantum-Zeno effect. Strictly following the principles of quantum mechanics one finds that the dynamics of a quantum system freezes when continuously measuring it with projective measurements [36–38]. This paradigm is particularly interesting in the context of the classical Maxwell demon, who continuously observes the system of its interest. Indeed, we find with the system and methods at hand that the action of the Maxwell demon results in a blocking of the particle and heat currents between the reservoirs.

Moreover, due to the action of the demon in the quantum regime, we observe another side effect. Besides building up a chemical potential gradient between the two reservoirs which could be used to charge a battery, we argue that there can be also a net energy decrease of the system due to the feedback action. We explain that it is most convenient to run the Maxwell demon in such a regime, as we do not have to invest external power in order to make the demon work.

This article is organized as follows: in section 2, we explain the SET, which we describe by a Fano–Anderson model. We give a compact introduction to the DCG method applied throughout the article and prove its validity. In section 3, we explain the implementation of the Maxwell demon by a piecewise-constant feedback scheme and show how to model this on the level of the equation of motion for the reduced density matrix. We show how the DCG approach reveals the quantum-Zeno effect for a continuous measurement. In section 4, we discuss the thermodynamic properties of the system like electric power, gain, heat flow and entropy production in the quantum-Zeno regime and beyond. In section 5, we provide a concluding discussion of our results. Supplemental information is given in the appendix.

2. Model and methods

We implement the Maxwell demon in a SET, which is a mesoscopic transport setup consisting of two electron reservoirs coupled by a quantum dot. A sketch of the system is depicted in figure 1(a). We model the SET by a two-terminal Fano–Anderson model, whose Hamiltonian reads [39–41]

$$\begin{aligned}\hat{H}^{\nu} &= \hat{H}_{\mathrm{d}} + \hat{H}_{\mathrm{r}} + \hat{H}_{\mathrm{c}}^{\nu},\\ \hat{H}_{\mathrm{d}} &= \epsilon\, \hat{c}_{\mathrm{d}}^{\dagger}\hat{c}_{\mathrm{d}},\\ \hat{H}_{\mathrm{r}} &= \sum_{k,\alpha=\mathrm{R,L}} \omega_{k,\alpha}\hat{c}_{k,\alpha}^{\dagger}\hat{c}_{k,\alpha} = \sum_{\alpha=\mathrm{R,L}} H_{\mathrm{r},\alpha},\\ \hat{H}_{\mathrm{c}}^{\nu} &= \sum_{k,\alpha=\mathrm{R,L}} t_{k,\alpha}^{\nu}(\hat{c}_{\mathrm{d}}^{\dagger}\hat{c}_{k,\alpha} + \mathrm{h.c.}) = \sum_{\alpha=\mathrm{R,L}} H_{\mathrm{c},\alpha}^{\nu},\end{aligned} \tag{1}$$

where $\hat{c}_{\mathrm{d}}^{\dagger}$ and $\hat{c}_{k,\alpha}^{\dagger}$ are fermionic operators representing the central dot with on-site energy ϵ and the reservoir states with energies $\omega_{k,\alpha}$, respectively. Thereby, $\alpha = \mathrm{R},\ \mathrm{L}$ (right, left) labels the reservoirs and k are their internal states. The hopping amplitudes between dot and reservoir states are given by $t_{k,\alpha}^{\nu}$.

We have introduced the index ν to implement a feedback protocol: the Hamiltonian (or more precisely the hopping amplitudes) will be conditioned on the dot occupation $\nu = \mathrm{E},\ \mathrm{F}$ (empty, filled). We provide more details in section 3.

The initial condition which we consider throughout the article is given by

$$\begin{aligned}\rho(0) &= \rho_{\mathrm{d}}^{0} \otimes \rho_{\mathrm{L}}(0) \otimes \rho_{\mathrm{R}}(0),\\ \rho_{\alpha}(0) &= \frac{1}{Z_{\alpha}}\mathrm{e}^{-\beta_{\alpha}(\hat{H}_{\mathrm{r},\alpha}-\mu_{\alpha}\hat{N}_{\mathrm{r},\alpha})},\end{aligned} \tag{2}$$

where ρ_{d}^{0} is the initial density matrix of the dot and $\rho_{\alpha}(0)$ are the initial density matrices of the reservoirs. Thus, the reservoirs are considered to be locally in a thermal equilibrium state with inverse temperatures $\beta_{\alpha} = 1/(k_{\mathrm{B}}T_{\alpha})$ and chemical potentials μ_{α}. Here, Z_{α} denotes the partition function which ensures that $\mathrm{Tr}\,[\rho_{\alpha}(0)] = 1$ and $\hat{N}_{\alpha} = \sum_{k}\hat{c}_{k\alpha}^{\dagger}\hat{c}_{k\alpha}$ is the particle number operator of the reservoir α.

In the following, we apply a DCG method [32] to calculate the dynamics of the reduced density matrix of the quantum dot $\rho_{\mathrm{d}}(t) = \mathrm{Tr}_{\mathrm{r}}[\rho(t)]$, where $\mathrm{Tr}_{\mathrm{r}}[.]$ denotes the trace over the reservoir degrees of freedom. We represent the reduced density matrix of the quantum dot in the local basis $|0\rangle = |\mathrm{vac}\rangle$ and $|1\rangle = \hat{c}_{\mathrm{d}}^{\dagger}|\mathrm{vac}\rangle$ and

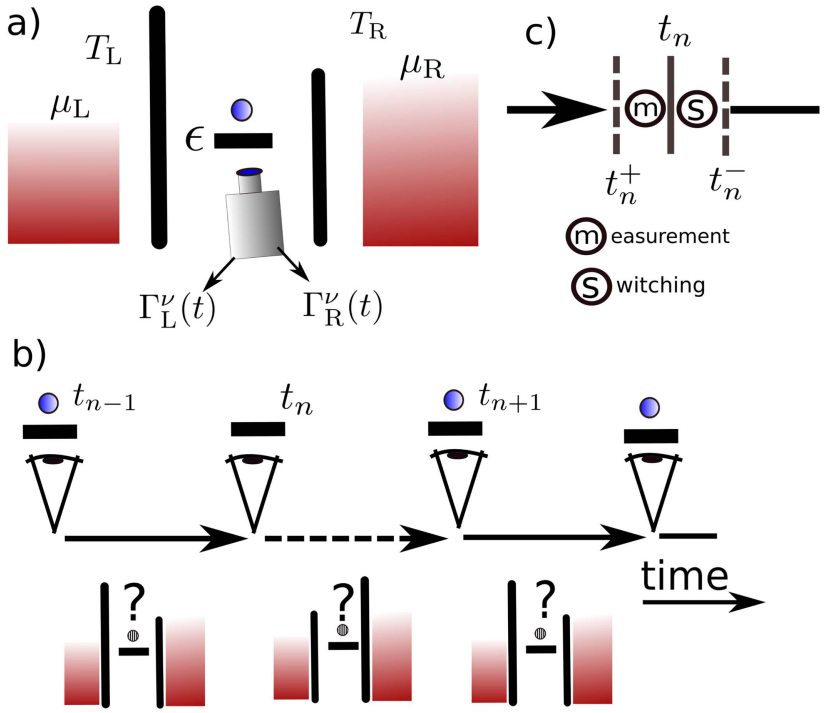

Figure 1. (a) Sketch of the SET under the action of the Maxwell demon. Two reservoirs, which are locally in thermal equilibrium, are connected via a quantum dot with on-site energy ϵ. The Maxwell demon monitors the occupation of the dot and adjusts the tunnel barriers $\Gamma^{\nu}_{\alpha}(t)$ according to its observation. In doing so, one can generate a current against the chemical potential bias even at equal temperatures. (b) As an implementation of the Maxwell demon, we consider a piecewise-constant feedback protocol. At times $t_n = n\tau$, we projectively measure the dot occupation $\nu = \mathrm{E},\ \mathrm{F}$ (empty, filled) using, e.g., a quantum-point contact. Subsequently, we adjust the tunnel rates accordingly for the next feedback period $(t_n,\ t_{n+1})$. On the level of equations we model this with the propagators $\exp[\mathcal{L}^{\tau}_{\nu}\tau]$ as explained in equation (15). (c) Temporal sketch of the feedback action in detail. The times t_n^-, t_n, t_n^+ denote the times (infinitesimally) before the measurement, after the measurement and after switching the tunnel rates, respectively.

introduce the notation $\rho_{\mathrm{d}},\ \lambda\lambda' \equiv \langle\lambda|\ \rho|\lambda'\rangle$. In doing so, the diagonal elements $\underline{\varrho} = (\rho_{\mathrm{d},00},\ \rho_{\mathrm{d},11})$ of the reduced density matrix of the system decouple from the coherences and approximately read as a function of time

$$\underline{\varrho}(t) = \exp\left[\sum_{\alpha=\mathrm{R,L}} \mathcal{L}^{t}_{\alpha,\nu}(\underline{\xi})t\right]\underline{\varrho}(0), \tag{3}$$

where the coarse-grained Liouvillian reads

$$\mathrm{L}^{t}_{\alpha,\nu}(\underline{\xi}) = \begin{pmatrix} -\gamma^{t,\alpha,\nu}_{10}(0) & \gamma^{t,\alpha,\nu}_{01}(\zeta_\alpha)\mathrm{e}^{\mathrm{i}\chi_\alpha} \\ \gamma^{t,\alpha,\nu}_{10}(\zeta_\alpha)\mathrm{e}^{-\mathrm{i}\chi_\alpha} & -\gamma^{t,\alpha,\nu}_{01}(0) \end{pmatrix}. \tag{4}$$

In equation (4) we additionally introduced the counting fields χ_α and ζ_α, which allow for a determination of the number of particles Δn_α and the amount of energy ΔE_α entering the reservoir α during the time interval $t' \in (0,\ t)$. For brevity we thereby combine the counting fields in the (transposed) vector $\underline{\xi}^T = (\chi_{\mathrm{L}},\ \chi_{\mathrm{R}},\ \zeta_{\mathrm{L}},\ \zeta_{\mathrm{R}})$. The matrix entries read

$$\begin{aligned} \gamma^{t,\alpha,\nu}_{10}(\zeta_\alpha) &= \frac{t}{2\pi}\int \mathrm{d}\omega \mathrm{sinc}^2\left[\frac{t}{2}(-\epsilon-\omega)\right]\gamma^{\alpha,\nu}_{10}(\omega)\mathrm{e}^{\mathrm{i}\zeta_\alpha\omega}, \\ \gamma^{t,\alpha,\nu}_{01}(\zeta_\alpha) &= \frac{t}{2\pi}\int \mathrm{d}\omega \mathrm{sinc}^2\left[\frac{t}{2}(\epsilon-\omega)\right]\gamma^{\alpha,\nu}_{01}(\omega)\mathrm{e}^{\mathrm{i}\zeta_\alpha\omega}, \end{aligned} \tag{5}$$

where $\mathrm{sinc}(x) \equiv \sin(x)/x$ is the sinc function and we have used the abbreviations

$$\gamma^{\alpha,\nu}_{10}(\omega) = \Gamma^{\nu}_{\alpha}(-\omega)f_\alpha(-\omega), \tag{6}$$

$$\gamma^{\alpha,\nu}_{01}(\omega) = \Gamma^{\nu}_{\alpha}(\omega)[1-f_\alpha(\omega)], \tag{7}$$

with the Fermi function $f_\alpha(\omega) = 1/(\mathrm{e}^{\beta_\alpha(\omega-\mu_\alpha)}+1)$ and the spectral coupling density $\Gamma_\alpha(\omega) = \sum_k |t^{\nu}_{k,\alpha}|^2\delta(\omega-\omega_{k,\alpha})$.

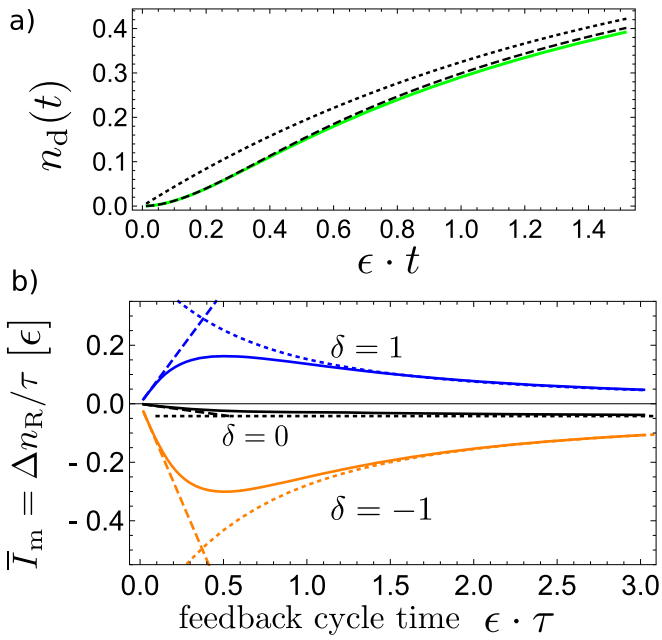

Figure 2. (a) Dot occupation $n_{\rm d}(t)$ as a function of time. The results of the DCG approach, the exact solution and the BMS master equation are depicted with a solid (green), dashed and dotted line, respectively. The parameters are $\Gamma^{\nu}_{0,\alpha} = 0.5\epsilon$, $\epsilon_{\rm L} = 5\epsilon$, $\epsilon_{\rm R} = -\epsilon$, $\delta_{\alpha} = 5\epsilon$, $\omega_{\rm max} = +\infty$, $\omega_{\rm min} = -\infty$, $\mu_{\rm L} = 0$, $\mu_{\rm L} = 10\epsilon$ and $T_{\rm L} = T_{\rm R} = 10\epsilon$. (b) Time-averaged currents $\overline{I}_{\rm m}$ under the action of the Maxwell demon in the stationary state as a function of the feedback time τ investigated in section 3. Overall parameters are as in panel (a) with $\Gamma^{\nu}_{0,\alpha} = 0.5\epsilon$, except that we have changed the cut-off frequencies to $\omega_{\rm max} = 20\epsilon$, $\omega_{\rm min} = 0$. The curves with feedback parameter $\delta = -1,\ 0,\ 1$ are depicted in blue, orange and black, respectively. The solid, dashed and dotted lines depict the solution with the DCG method, the linear expansion for short times τ and the BMS master equation result, respectively.

In the numerical calculations throughout the article, we use

$$\Gamma^{\nu}_{\alpha}(\omega) = \Gamma^{\nu}_{0,\alpha} \frac{\delta_{\alpha}^2 \Theta(\omega - \omega_{\rm min})\Theta(\omega_{\rm max} - \omega)}{(\omega - \epsilon_{\alpha})^2 + \delta_{\alpha}^2}. \tag{8}$$

This is a Lorentz function which is centered around ϵ_{α} and has a width δ_{α}. The function $\Theta(x)$ is the Heavyside function which ensures a compact support of the spectral coupling density between $\omega_{\rm min}$ and $\omega_{\rm max}$ needed for numerical calculations.

In figure 2(a), the accuracy of the DCG method is benchmarked against the exact solution of the Fano–Anderson model in the absence of feedback action [40]. There, we depict the occupation of the dot, which is given by $n_{\rm d}(t) = \rho_{{\rm d},11}(t)$. The DCG approach is optimized to resemble the exact dynamics for short times t [28, 32], see figure 2(a). By construction, in the long-time limit $t \to \infty$ the DCG dynamics converges to the dynamics of the Born–Markov-secular (BMS) master equation, which resembles the exact solution for the parameters under consideration. Consequently, the DCG method guarantees a good performance for short times in all parameter regimes and for long times in the weak-coupling limit. Importantly, due to its construction, the DCG method maintains a Lindblad form in equation (4) for all times t, which ensures positivity of $\rho_{\rm d}$ and consequently guarantees well-defined thermodynamic calculations.

Importantly, in the derivation of the DCG method it is assumed that the initial state is a product state of the central system and the reservoirs, which are assumed to be locally in a thermal equilibrium state [32]. As we explain below, this requirement is met for the feedback scheme which we apply here.

3. Feedback control

In order to implement the Maxwell demon we apply a projective measurement in combination with a piecewise-constant feedback scheme. This is sketched in figure 1(b). At times $t_n = n\tau$ we conduct projective measurements of the dot occupation. According to the outcome, we adjust the system parameters which then remain constant for the following time interval $t \in (t_n,\ t_{n+1})$. In particular, here we vary the tunnel barriers which are parameterized by $\Gamma^{\nu}_{\alpha}(\omega)$ with $\nu = {\rm E},\ {\rm F}$ if the dot occupation has been empty or filled at time t_n, respectively.

3.1. Action on the density matrix of the total system

The feedback interventions occur at times $t_n = n\tau$. Within the time intervals $(t_n,\ t_{n+1})$ the total system (including the reservoirs) evolves under the Hamiltonian equation (1) conditioned on $\nu = \mathrm{E},\ \mathrm{F}$ and is therefore conservative. The total energy can thus only change during the feedback interventions at times $t_n = n\tau$.

The intervention can be divided in two steps. To this end, we introduce the (virtual) times t_n^+ and t_n^- as depicted in figure 1(c) for illustration. First, one has to measure the dot occupation. This measurement shall take place during the time interval $(t_n^-,\ t_n)$. Is it know that a projective measurement can change the mean energy of the system [42–44], which can even give rise to measurement induced extracted work in a Maxwell demon setup [45].

Second, according to the measurement outcome, we adjust the tunnel barriers $\Gamma_\alpha^\nu(\omega)$. This step shall take place in the time interval $(t_n,\ t_n^+)$. However, as we explain in section 4.2, for projective measurements the switching work can be here neglected, such that only the first step changes the energy of the total system.

As the total Hamiltonian equation (1) is quadratic, the most important observables as the total system energy can be determined by the single-particle density matrix

$$\rho_{x,y} = \mathrm{Tr}\,[\hat{c}_x^\dagger \hat{c}_y \rho], \tag{9}$$

with $x,\ y \in \{\mathrm{d},\ (k,\ \alpha)\}$.

The projectors which project the system state to the empty and filled quantum dot are given by

$$\hat{P}_\mathrm{E} = \hat{c}_\mathrm{d}\hat{c}_\mathrm{d}^\dagger, \qquad \hat{P}_\mathrm{F} = \hat{c}_\mathrm{d}^\dagger \hat{c}_\mathrm{d}. \tag{10}$$

Their action on the total system density matrix is accordingly [46]

$$\rho(t_n^-) \to \rho^\nu(t_n) = \frac{\hat{P}_\nu \rho(t_n^-)\hat{P}_\nu}{\mathrm{Tr}\,[\hat{P}_\nu \rho(t_n^-)]}. \tag{11}$$

In consequence, it is easy to see that the single-particle density matrix elements become $\rho_{\mathrm{d,d}} \to \{0,\ 1\}$ and $\rho_{\mathrm{d},(\mathrm{k},\alpha)} \to 0$. The two distinct measurement results $\nu = \mathrm{E},\ \mathrm{F}$ can be found with probabilities $p_\nu = \mathrm{Tr}\,[\hat{P}_\nu \rho(t_n^-)]$, so that the density matrix of the total system after the measurement irrespective of the measurement outcome reads

$$\rho(t_n) = \sum_{\nu=\mathrm{E,F}} p_n \rho^\nu(t_n) = \sum_{\nu=\mathrm{E,F}} \hat{P}_\nu \rho(t_n^-)\hat{P}_\nu. \tag{12}$$

In the subsequent time interval $(t_n^+,\ t_{n+1}^-)$, the dynamics is determined by the Hamiltonian $\hat{H}^\nu$ depending on the measurement result $\nu = \mathrm{E},\ \mathrm{F}$. Importantly, $\rho_{\mathrm{d},(\mathrm{k},\alpha)} \to 0$ means that there are no system-reservoir coherences after the measurement. This is essential for the application of the DCG method in the subsequent time evolution.

3.2. Time evolution of the reduced density matrix

In the following, we describe the dynamics on the level of the reduced density matrix of the quantum dot ρ_d. For its diagonal elements contained in the vector $\underline{\varrho}$, the projective measurement in equation (11) translates into

$$\hat{P}_\nu \rho \hat{P}_\nu \quad \hat{=} \quad \boldsymbol{\mathcal{P}}_\nu \underline{\varrho}, \tag{13}$$

where

$$\boldsymbol{\mathcal{P}}_\mathrm{E} = \begin{pmatrix} 1 & 0 \\ 0 & 0 \end{pmatrix}, \qquad \boldsymbol{\mathcal{P}}_\mathrm{F} = \begin{pmatrix} 0 & 0 \\ 0 & 1 \end{pmatrix}, \tag{14}$$

are the measurement operators corresponding to the measurement results $\nu = \mathrm{E},\ \mathrm{F}$.

The projective measurement is subsequently followed by a time evolution which is conditioned on the measurement result. The conditioned time evolution can be described by the DCG approach in equation (3), so that the feedback time-evolution propagator reads [47]

$$\boldsymbol{\mathcal{F}}^\tau(\underline{\xi}) = \mathrm{e}^{\boldsymbol{\mathcal{L}}_\mathrm{E}^\tau(\underline{\xi})\tau}\boldsymbol{\mathcal{P}}_\mathrm{E} + \mathrm{e}^{\boldsymbol{\mathcal{L}}_\mathrm{F}^\tau(\underline{\xi})\tau}\boldsymbol{\mathcal{P}}_\mathrm{F}, \tag{15}$$

where $\boldsymbol{\mathcal{L}}_\nu^\tau(\underline{\xi}) = \sum_\alpha \boldsymbol{\mathcal{L}}_{\alpha,\nu}^\tau(\underline{\xi})$. The propagator $\boldsymbol{\mathcal{F}}^\tau(\underline{\xi})$ evolves the reduced density matrix by one feedback period τ. We emphasize that the repeated application of the propagator is in agreement with the derivation of the DCG method, which assumed that the initial condition is given by a product state of system and reservoir density matrices. This requirement is fulfilled, as the projective measurements result in a destruction of the system-reservoir correlations as explained in section 3.1.

From the generalized propagator $\boldsymbol{\mathcal{F}}^\tau(\underline{\xi})$ we obtain the moment generation function (MGF)

$$M(\tau,\ \underline{\xi}) = (1,\ 1)\boldsymbol{\mathcal{F}}^\tau(\underline{\xi})\underline{\varrho}_\mathrm{s}, \tag{16}$$

where $\underline{\varrho}_\mathrm{s}$ denotes the stationary density matrix, as we are interested in the long-term dynamics. The stroboscopic stationary state at times $t_n = n\tau$ is the eigenvector of $\boldsymbol{\mathcal{F}}^\tau(0)$ with eigenvalue $\varphi_1 = 1$,

$$\mathcal{F}^{\tau}(0)\,\underline{\varrho}_{\mathrm{s}} = \underline{\varrho}_{\mathrm{s}}, \tag{17}$$

which always exists and depends on the measurement rate τ. Furthermore, it can be shown that the second eigenvalue fulfills $0 \leqslant \varphi_2 \leqslant 1$. It thus describes the relaxation dynamics towards the stationary state. In terms of the MGF, the number of particles entering reservoir α within the time interval τ is given by [29]

$$\Delta n_{\alpha} = -\mathrm{i}\frac{\mathrm{d}}{\mathrm{d}\chi_{\alpha}} M(\tau, \underline{\xi})|_{\underline{\xi}=0}. \tag{18}$$

In the same way we obtain the change of energy ΔE_{α} in reservoir α by deriving $M(\tau, \underline{\xi})$ with respect to ζ_{α} instead.

In figure 2(b), we depict the time-averaged matter current $\overline{I}_{\mathrm{m}} = \Delta n_{\mathrm{R}}/\tau = -\Delta n_{\mathrm{L}}/\tau$ as a function of τ. In doing so, we have chosen the parametrization of the spectral coupling density as in equation (8), but with the proportional parameter adjusted to

$$\begin{aligned} \Gamma^{\nu}_{0,\mathrm{L}} &\to \begin{cases} \Gamma_{0,\mathrm{L}}\mathrm{e}^{+\delta} & \nu = \mathrm{E} \\ \Gamma_{0,\mathrm{L}}\mathrm{e}^{-\delta} & \nu = \mathrm{F}, \end{cases} \\ \Gamma^{\nu}_{0,\mathrm{R}} &\to \begin{cases} \Gamma_{0,\mathrm{R}}\mathrm{e}^{-\delta} & \nu = \mathrm{E} \\ \Gamma_{0,\mathrm{R}}\mathrm{e}^{+\delta} & \nu = \mathrm{F} \end{cases}. \end{aligned} \tag{19}$$

The parameter δ controls the feedback action. For $\delta = 0$, there is no feedback control. For $\delta > 0$, the feedback control supports a matter current from the left to the right reservoir, while for $\delta < 0$ the feedback supports the opposite direction.

We depict $\overline{I}_{\mathrm{m}}$ for three different feedback strengths δ with solid lines. Here and in the following, we choose equal temperatures $T_{\mathrm{L}} = T_{\mathrm{R}} = T$ in order to exclude a thermoelectric effect [40]. For the chemical potentials we consider $\mu_{\mathrm{L}} < \mu_{\mathrm{R}}$. Consequently, the time-averaged current $\overline{I}_{\mathrm{m}}$ is negative in the absence of feedback, as can be found for $\delta = 0$. For a positive feedback parameter $\delta = 1$, we can find a current against the bias $V = \mu_{\mathrm{L}} - \mu_{\mathrm{R}}$ and we generate a time-averaged electric power, which we define as

$$\overline{P} \cdot \tau = -\Delta n_{\mathrm{R}} \cdot V. \tag{20}$$

Using this definition, we generate electric power for $\overline{P} > 0$ and waste power for $\overline{P} < 0$. For $\delta < 0$, our numerical calculations verify that the feedback protocol supports the current along the chemical potential bias.

For long feedback times $\tau \to \infty$ the time-averaged current is always directed along the chemical potential bias irrespective of the feedback strength δ. This can be explained as follows. In the limit of long feedback times τ, the dynamics of the propagators conditioned on $\nu = \mathrm{E}, \mathrm{F}$ in equation (15) converges to the ones of the BMS master equation, respectively [28]. Regardless of the feedback time τ, the propagator in equation (15) describes an average of two distinct time evolutions with no feedback. For the BMS master equation (in the absence of feedback and at equal temperatures) it is known that the current always flows along the chemical potential bias in the long-time limit. This is a consequence of the second law of thermodynamics which is respected by the BMS master equation. Consequently, the measurement-averaged current becomes directed along the chemical potential gradient.

3.3. Maxwell demon in the quantum-Zeno regime

In the limit of continuous feedback $\tau \to 0$, the current vanishes independent of the feedback parameter δ as can be observed in figure 2(b). This can be explained with the quantum-Zeno effect. For $\tau = 0$, the propagator calculated using the DCG approach in equation (15) becomes

$$\mathcal{F}^{0}(\underline{\xi}) = \begin{pmatrix} 1 & 0 \\ 0 & 1 \end{pmatrix}. \tag{21}$$

This means that now both eigenvalues are $\varphi_{\lambda} = 1$. As a consequence, the system is now bistable: Either the dot is occupied or empty for all times. In addition, coherences are continuously projected to zero as discussed in section 3.1. Due to the infinite measurement rate, the dot dynamics gets thus frozen, so that no particle can enter or leave the reservoirs. Thus, the DCG method under consideration resembles the quantum-Zeno effect [36–38].

Here, the Zeno suppression is solely induced by frequent projective measurements. By contrast, there is also the possibility to generate a Zeno effect by increasing the decoherence rate by increasing the coupling to the reservoirs as discussed in [48–50]. In the DCG approach applied here, this effect is absent, as we treat the coupling to the reservoirs in lowest order (e.g., in the strong-coupling regime the treatment is only valid for very short coarse-graining times).

In order to find a compact approximation and an intuitive explanation for the behavior in the quantum-Zeno regime, we expand the MGF for short times up to the lowest non-vanishing order in τ which still contains a dependence on the counting field. In doing so, we find

$$M(\chi, \tau) = (1, 1)(1 + \boldsymbol{\mathcal{L}}_{\mathrm{E}}(\chi)\tau^2\boldsymbol{\mathcal{P}}_{\mathrm{E}} + \boldsymbol{\mathcal{L}}_{\mathrm{F}}(\chi)\tau^2\boldsymbol{\mathcal{P}}_{\mathrm{F}} + ...)(\underline{\varrho}_{s,0} + ...), \tag{22}$$

where we have defined

$$\boldsymbol{\mathcal{L}}_{\nu}(\underline{\xi}) = \sum_{\alpha=\mathrm{R,L}} \begin{pmatrix} -g_{10}^{\alpha,\nu}(0) & g_{01}^{\alpha,\nu}(\zeta_\alpha)\mathrm{e}^{\mathrm{i}\chi_\alpha} \\ g_{10}^{\alpha,\nu}(\zeta_\alpha)\mathrm{e}^{-\mathrm{i}\chi_\alpha} & -g_{01}^{\alpha,\nu} \end{pmatrix}, \tag{23}$$

and

$$g_{10}^{\alpha,\nu}(\zeta_\alpha) = \frac{1}{2\pi}\int \mathrm{d}\omega \Gamma_\alpha^\nu(\omega)\mathrm{e}^{-\mathrm{i}\zeta_\alpha\omega} f_\alpha(\omega), \tag{24}$$

$$g_{01}^{\alpha,\nu}(\zeta_\alpha) = \frac{1}{2\pi}\int \mathrm{d}\omega \Gamma_\alpha^\nu(\omega)\mathrm{e}^{\mathrm{i}\zeta_\alpha\omega}[1 - f_\alpha(\omega)]. \tag{25}$$

We note that the spectral coupling density $\Gamma_\alpha^\nu(\omega)$ must ensure an appropriate frequency cut-off in order to avoid that higher derivatives with respect to ζ_α diverge. The MGF in the short feedback time limit thus reads

$$\begin{aligned} m(\underline{\xi}, \tau) = \tau^2 \sum_{\alpha=\mathrm{R,L}} & n_{\mathrm{s},0} g_{01}^{\alpha,\mathrm{F}}(\xi_\alpha)\mathrm{e}^{-\mathrm{i}\chi_\alpha} \\ & + (1 - n_{\mathrm{s},0}) g_{10}^{\alpha,\mathrm{E}}(\xi_\alpha)\mathrm{e}^{\mathrm{i}\chi_\alpha}, \end{aligned} \tag{26}$$

where

$$n_{\mathrm{s}} \to n_{\mathrm{s},0} = \frac{1}{1 + \frac{g_{01}^{\mathrm{L,F}}(0) + g_{01}^{\mathrm{R,F}}(0)}{g_{10}^{\mathrm{L,F}}(0) + g_{10}^{\mathrm{R,F}}(0)}} \tag{27}$$

denotes the corresponding occupation of the dot. We emphasize that the first non-vanishing order of the MGF is $\propto\tau^2$. In consequence, the time-averaged current $\overline{I}_{\mathrm{m}} = \Delta n_{\mathrm{R}}/\tau$ and all higher cumulants vanish for $\tau \to 0$. This τ^2 behavior is a typical feature in the Zeno regime [37].

Generally, the BMS master equation results are not valid in the short-time regime. A short-time expansion as before reveals why the BMS treatment provides an inaccurate result as can be seen in figure 2(b). Formally, the time evolution of the BMS approach reads as in equation (3), but with the time-dependent matrices replaced by time-independent ones, thus $\boldsymbol{\mathcal{L}}_\alpha^\tau \to \boldsymbol{\mathcal{L}}_\alpha^{\mathrm{BMS}}$. Performing the same expansion of the MGF, we find that $M(\underline{\zeta}, \tau) \propto \tau$. Consequently, the Born–Markov treatment leads to a finite time-averaged current $\overline{I}_{\mathrm{m}}$ even for vanishing feedback times.

Let us choose a positive feedback strength δ which implies a current against the bias for rather short τ, thus $\overline{I}_{\mathrm{m}}(\tau) > 0$. As we explained in section 3.2 , for long feedback periods τ the current flows always along the chemical potential gradient, thus $\overline{I}_{\mathrm{m}}(\tau) < 0$. Then there must be consequently a feedback time τ_0 at which the time-averaged current vanishes, thus $\overline{I}_{\mathrm{m}}(\tau_0) = 0$. As $\overline{I}_{\mathrm{m}}(0) = 0$ due to the Zeno effect, it is also clear that there must be a feedback time τ in the interval $(0, \tau_0)$ at which the current against the chemical potential reaches a maximum value, as can be seen in figure 2(b).

4. Power, gain and heat flow

4.1. Power

In figure 3(a), we depict the power as a function of the bias $V = \mu_{\mathrm{L}} - \mu_{\mathrm{R}}$ and the feedback time τ. The dashed lines depict levels of equal power. The solid lines show the set of $\overline{P} = 0$. There are two ways to cross this boundary. At the line $V = 0$ the bias changes sign, while in the upper left region of the diagram there is a sign change of $\overline{P}$ as the time-averaged current $\overline{I}_{\mathrm{m}}$ changes its direction. Overall, the power is close to zero in wide parts of the diagram, but shows more structure for small τ. Here, we see that the feedback scheme generates most power for large negative bias and intermediate feedback times $\epsilon\tau \approx 0.5$. On the other hand, most power is wasted for a large positive power and an intermediate feedback time.

4.2. Gain

In order to estimate the performance of Maxwell's demon, power is not the only decisive quantity. As the total process is not conservative, the energy of the total system changes. In particular, we find that the total energy can increase or even decrease on average. This amount of energy change is denoted with feedback energy ΔE_{fb} in the following. For $\Delta E_{\mathrm{fb}} > 0$, the action of the Maxwell demon leads to an increase of the total system energy, while for $\Delta E_{\mathrm{fb}} < 0$, the total system energy decreases. We define the corresponding gain parameter

$$G = \frac{\overline{P}\cdot\tau}{\Delta E_{\mathrm{fb}}} \cdot \Theta(\overline{P}) \cdot \Theta(\Delta E_{\mathrm{fb}}), \tag{28}$$

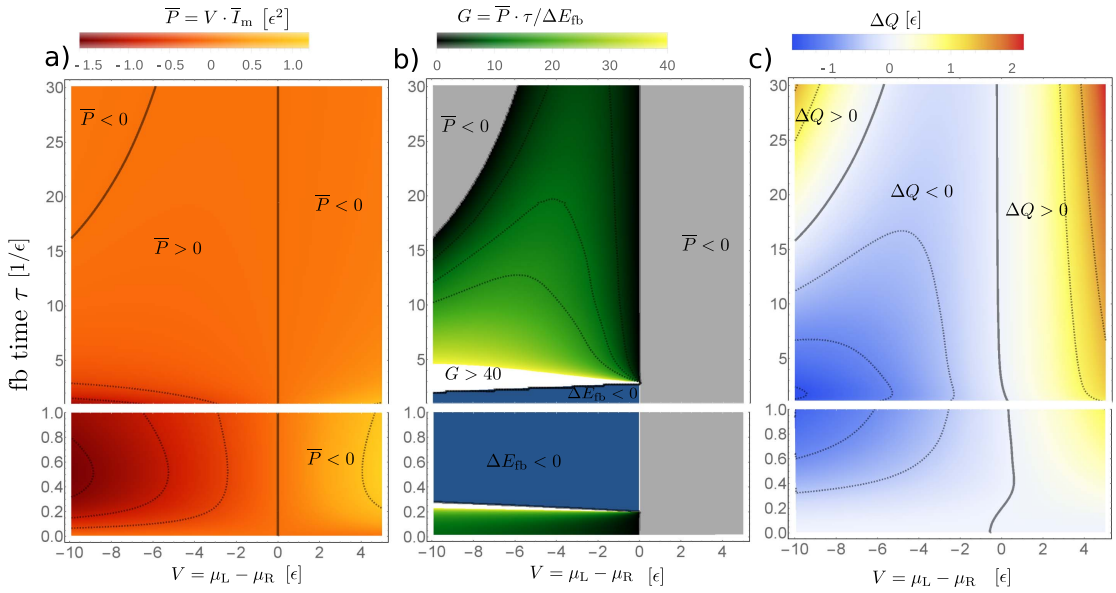

Figure 3. (a) Time-averaged power $\overline{P}$ as a function of the chemical potential bias V and the feedback time τ. Dashed lines depict sets of equal power. The solid lines mark the set with $\overline{P} = 0$. Overall parameters are as in figure 2(b) with $\delta = 1$. (b) Depicts the corresponding gain defined in equation (28). In the gray region we find $\overline{P} < 0$ and the gain is not interesting as we waste power. In the white region we find $G > 40$. The most efficient way to run the Maxwell demon is in the blue region, where $\Delta E_{\mathrm{fb}} < 0$ so that one does not have to invest power to run the feedback protocol. (c) Total amount of heat ΔQ defined in equation (36) which enters ($\Delta Q > 0$) or leaves ($\Delta Q < 0$) the reservoirs. The solid lines mark the set with $\Delta Q = 0$. The regions of $\Delta Q < 0$ are strongly correlated to the regions of $\overline{P} > 0$.

where we restrict the definition of the gain to positive power $\overline{P} > 0$ and feedback energy $\Delta E_{\mathrm{fb}} > 0$. The feedback energy can be calculated by considering in detail the feedback process as sketched in figures 1(b), (c) and explained in section 3.1.

We first determine the change of the mean energy of the total system due to the measurement in the virtual time interval $t \in (t_n^-, t_n)$. To this end, we have to determine the difference of the energies of the total system in equation (1) before and after the measurement,

$$\Delta E_{\mathrm{tot}}^{\nu}[\rho(t_n^-)] = \mathrm{Tr}[\hat{H}^{\nu}\rho(t_n)] - \mathrm{Tr}[\hat{H}^{\nu}\rho(t_n^-)]. \tag{29}$$

Thus, we compare the energy of the state shortly before the measurement $\rho(t_n^-)$ with the state after the measurement $\rho(t_n)$ with regard to the total Hamiltonian before the measurement. As theses density matrices differ only in the dot-reservoir coherences $\rho_{\mathrm{d},(k,\alpha)}$, which vanish due to the measurement $\rho_{\mathrm{d},(k,\alpha)}(t_n) \to 0$, we find

$$\Delta E_{\mathrm{tot}}^{\nu}[\rho(t_n^-)] = \langle \hat{H}_{\mathrm{c}}^{\nu} \rangle_{t_n^-}, \tag{30}$$

where we have introduced the notation

$$\langle \hat{O} \rangle_t \equiv \mathrm{Tr}[\hat{O}\rho(t)]. \tag{31}$$

This can be evaluated as follows

$$\begin{aligned} \Delta E_{\mathrm{tot}}^{\nu}[\rho(t_n^-)] &= -\langle \hat{H}^{\nu} - \hat{H}_{\mathrm{d}} - \hat{H}_{\mathrm{r}} \rangle_{t_n^-} \\ &= -\langle \hat{H}^{\nu} \rangle_{t_{n-1}^+} + \langle \hat{H}_{\mathrm{d}} + \hat{H}_{\mathrm{r}} \rangle_{t_n^-} \\ &= -\langle \hat{H}_{\mathrm{d}} + \hat{H}_{\mathrm{r}} \rangle_{t_{n-1}^+} + \langle \hat{H}_{\mathrm{d}} + \hat{H}_{\mathrm{r}} \rangle_{t_n^-} \\ &\equiv \Delta E_{\mathrm{d}}^{\nu} + \Delta E_{\mathrm{r}}^{\nu}. \end{aligned} \tag{32}$$

From line one to line two we have used that the total system evolves under a conservative time evolution in the interval (t_{n-1}^+, t_n^-). Line two is equal to line three as there are no dot-reservoir coherences at time t_{n-1}^+. Finally in line four, we have defined the energy differences corresponding to the dot and reservoir subsystem, respectively, thus $\Delta E_{\mathrm{d}}^{\nu} \equiv \langle \hat{H}_{\mathrm{d}} \rangle_{t_n^-} - \langle \hat{H}_{\mathrm{d}} \rangle_{t_{n-1}^+}$, and accordingly for $\Delta E_{\mathrm{r}}^{\nu}$.

Equation (32) is an interesting result, as it relates the change of energy induced by the measurement at time $t = t_n$ with the energy-conserving time evolution in the preceding time interval (t_{n-1}^+, t_n^-). We emphasize that this result is exact and holds even for more complicated Hamiltonians under the assumption that all system-reservoir coherences vanish due to the projective measurement.

If we consider a stationary state which is characterized by $\rho_{\mathrm{d,d}}(t_{n-1}) = \rho_{\mathrm{d,d}}(t_n)$, we find for the averaged energy change

$$\Delta E_{\mathrm{fb}} = \sum_{\nu=\mathrm{E,F}} p_{\mathrm{s},\nu} \Delta E^{\nu}_{\mathrm{tot}}[\rho^{\nu}_{\mathrm{s}}(t_n^-)], \tag{33}$$

where $\rho^{\nu}_{\mathrm{s}}(t_n^-)$ is the density matrix if the measurement outcome at time t_{n-1} has been ν. The corresponding probability is denoted by $p_{\mathrm{s},\nu}$. In the stationary state, the averaged dot energy is constant at times t_n, so that we find

$$\Delta E_{\mathrm{fb}} = \sum_{\nu=\mathrm{E,F}} p_{\mathrm{s},\nu} \,\mathrm{Tr}\,\{\hat{H}_{\mathrm{r}}[\rho^{\nu}_{\mathrm{s}}(t_n^-) - \rho^{\nu}_{\mathrm{s}}(t_{n-1}^+)]\}. \tag{34}$$

This is the energy entering the reservoir during the interval (t_{n-1}^+, t_n^-) averaged over the measurement results ν in the stationary state. Using the DCG method, we can thus obtain the feedback energy ΔE_{fb} by deriving the MGF

$$\begin{aligned}\Delta E_{\mathrm{fb}} &= -\mathrm{i} \sum_{\alpha=\mathrm{L,R}} \frac{\mathrm{d}}{\mathrm{d}\zeta_\alpha} M(\tau, \underline{\xi})|_{\underline{\xi}=0} \\ &\equiv \Delta E_{\mathrm{L}} + \Delta E_{\mathrm{R}},\end{aligned} \tag{35}$$

where we have finally partitioned the total energy change into energies entering the left ΔE_{L} and right ΔE_{R} reservoirs within the feedback period τ. We note, that this result is consistent with the first law of thermodynamics.

In figure 3(b) we depict the gain G in the same regime as in (a) where we generate power, $\overline{P} > 0$. For regions where $\Delta E_{\mathrm{fb}} > 0$ we use a color code. For a clear representation, we restrict the range to $G \in (0,\ 40)$. In the blue regions, we find a negative feedback energy $\Delta E_{\mathrm{fb}} < 0$, thus, the total system energy decreases due to the measurement and the demon does not perform work on the system but extracts work. It is thus most profitable to operate the system in this region.

Close to the transition at $\Delta E_{\mathrm{fb}} = 0$ the gain diverges. This line represents the original idea of the Maxwell demon that due to a energy conserving action of the demon (measurement, opening and closing the door) one can generate a thermal gradient or increase a chemical potential bias. However, we emphasize that even though in the quantum regime the measurement does not change the energy balance, it changes the state of the system. This is in contrast to the classical Maxwell demon, where the measurement leaves the system state unaffected.

In principle, one could argue that a negative feedback energy $\Delta E_{\mathrm{fb}} < 0$ could be stored or used by a smart demon for another application. However, a detailed discussion of this issue could become possible when specifying the measurement apparatus [51–53].

4.3. Heat, entropy and information efficiency

Next we discuss the heat flow and the thermodynamic consistency. In the stationary state, the change of heat entering the reservoirs within a feedback period τ reads

$$\begin{aligned}\Delta Q &= \Delta Q_{\mathrm{L}} + \Delta Q_{\mathrm{R}}, \\ \Delta Q_\alpha &= \Delta E_\alpha - \mu_\alpha \Delta n_\alpha.\end{aligned} \tag{36}$$

The heat is depicted in figure 3(c). The solid curves represent sets where the total heat change in the reservoirs vanishes $\Delta Q = 0$. These curves resemble roughly the zero power curves $\overline{P} = 0$. A power generation is thus correlated to an overall loss of heat in the reservoirs. The correlation of $\Delta Q = 0$ and $\overline{P} = 0$ becomes clear when considering the relation

$$\begin{aligned}\Delta Q &= \Delta E_{\mathrm{L}} + \Delta E_{\mathrm{R}} + \Delta n_{\mathrm{R}}(\mu_{\mathrm{L}} - \mu_{\mathrm{R}}) \\ &= \Delta E_{\mathrm{fb}} - \overline{P} \cdot \tau.\end{aligned} \tag{37}$$

As ΔE_{fb} is small compared to $\overline{P} \cdot \tau$ for a wide parameter range (compare with figure 3(b)), we find $\Delta Q \approx -\overline{P} \cdot \tau$, which explains the correspondence of the curves $\Delta Q = 0$ and $\overline{P} = 0$.

The second law of thermodynamics says that on average the total entropy increases in time in the absence of feedback processes. In a stationary state, this relation reads

$$\Delta S_{\mathrm{i}} = \Delta S + \Delta S_{\mathrm{e}} \geqslant 0, \tag{38}$$

where ΔS_{i} denotes the entropy production and ΔS_{e} is the entropy change in the reservoirs within a time interval τ. The change of entropy in the system (i.e., quantum dot) is given by

$$\begin{aligned}\Delta S &= S(t+\tau) - S(t), \\ S(t) &= -k_{\mathrm{B}} \,\mathrm{Tr}\,[\rho_{\mathrm{d}}(t) \ln \rho_{\mathrm{d}}(t)].\end{aligned} \tag{39}$$

In [54], Esposito and coworkers have derived a general relation for the entropy change which is valid for arbitrary system-reservoir setups. Under the assumption of a product initial state as in equation (2) and a unitary time evolution, the entropy change in the reservoirs reads

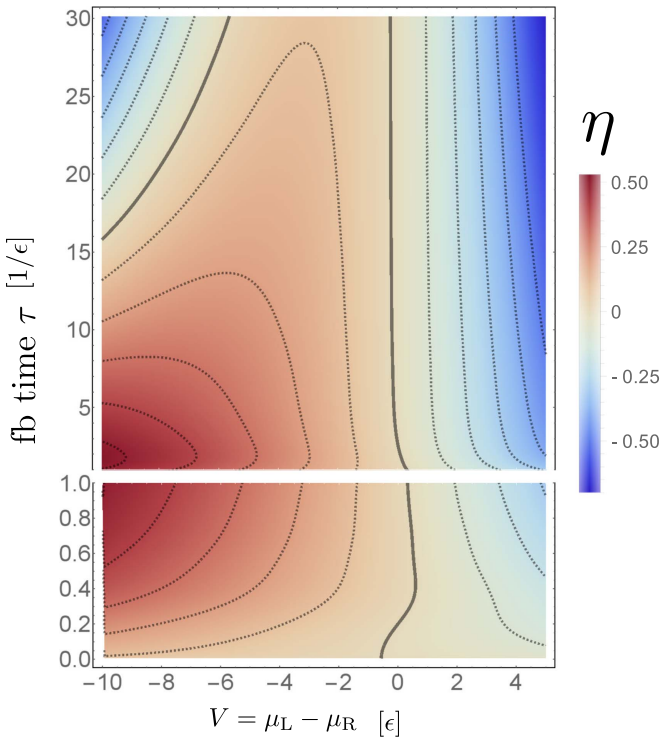

Figure 4. (a) Information efficiency η as defined in equation (42). The parameters are as in figure 3.

$$\Delta S_e = \sum_\alpha \beta_\alpha \Delta Q_\alpha. \tag{40}$$

Similar considerations can be found in [12, 55, 56]. It is straightforward to generalize this to the feedback protocol considered here. To this end, we consider the change of entropy conditioned on the measurement outcome at time $t = t_n$ within the subsequent feedback period $t \in (t_n^+, t_{n+1}^-)$. For both measurement outcomes the second law in equation (38) together with equation (40) is fulfilled separately, so that we find for the measurement-averaged entropy change

$$\Delta\tilde{S} + \Delta\tilde{S}_e \equiv \sum_{\nu=E,F} p_\nu \Delta S^{(\nu)} + \sum_{\nu=E,F} p_\nu \Delta S_e^{(\nu)} \geqslant 0. \tag{41}$$

The action of the measurement is to delete the entropy of the system by exactly the amount $\mathcal{I} = -\Delta\tilde{S}$ during the virtual time interval (t_{n+1}^-, t_{n+1}) [7]. For this reason, one can interpret equation (41) in the following way: the amount of entropy reduced by the measurement is not completely transferred to the reservoirs [57]. Moreover, it is not hard to prove that $\Delta\tilde{S} \leqslant k_B \ln 2$, so that we recover the Landauer principle [6].

Equation (41) allows to define a coefficient which measures how efficient the information is used to decrease the entropy in the reservoir

$$\eta = \frac{\Delta\tilde{S}_e}{I} \leqslant 1, \tag{42}$$

which we denote as information efficiency in the following [16]. While $\mathcal{I} < 0$, the entropy change in the reservoir $\Delta\tilde{S}_e$ can be both, positive or negative, so that the information efficiency is not bounded from below. For similar inequalities in other feedback systems we refer to [58, 59].

We depict η in figure 4. We observe that the information efficiency is bounded by $\eta \leqslant 1$, which is a sanity check for the applied DCG method. The information efficiency is rather similar to the heat ΔQ entering the reservoirs. This is a consequence of the dot occupation, which is approximately $n_s = p_F \approx 0.5$ for the considered parameters.

4.4. Feedback energy and gain in the Zeno regime

As the general expression for the matter and energy current is rather involved, it is hard to understand under which circumstances the feedback energy is small or even negative. For this reason, we focus on the Zeno regime in the following, where the expressions are simpler. In this regime, the feedback energy reads

$$\Delta E_{\mathrm{fb}} = \tau^2 \sum_{\alpha=\mathrm{R,L}} [n_{\mathrm{s},0}\tilde{g}_{01}^{\alpha,\mathrm{F}} + (1-n_{\mathrm{s},0})\tilde{g}_{10}^{\alpha,\mathrm{E}}], \tag{43}$$

where $\tilde{g}_{xy}^{\alpha,\nu} = \partial_{\zeta_\alpha} g_{xy}^{\alpha,\nu}|_{\underline{\zeta}=0}$. In order to keep the analysis simple, we focus on an extremal feedback case where $\Gamma_{\mathrm{L}}^{\mathrm{F}}(\omega) = \Gamma_{\mathrm{R}}^{\mathrm{E}}(\omega) = 0$. In most cases we numerically find that the stationary dot occupation is close to $n_{\mathrm{s},0} \approx 0.5$, so that we find a small or negative current if $\tilde{g}_{01}^{\mathrm{R,F}} < \tilde{g}_{10}^{\mathrm{L,E}}$. This relation implies

$$\tilde{\Delta} \equiv \int \mathrm{d}\omega \Gamma_{\mathrm{R}}^{\mathrm{F}}(\omega)\omega[1-f_{\mathrm{R}}(\omega)] - \Gamma_{\mathrm{L}}^{\mathrm{E}}(\omega)\omega f_{\mathrm{L}}(\omega) < 0. \tag{44}$$

This condition can be met if the temperatures in the reservoirs are rather high $\beta_\alpha \epsilon \ll 1$, so that the Fermi functions are rather close to $f_\alpha(\omega) \approx 0.5$ around a broad range around $\omega = \mu_\alpha$. If additionally $\Gamma_{\mathrm{L}}^{\mathrm{E}}(\omega)$ is large for large ω and $\Gamma_{\mathrm{R}}^{\mathrm{F}}(\omega)$ is large for small ω, the quantity $\tilde{\Delta}$ and consequently also the feedback energy ΔE_{fb} can become rather small or even negative.

This is exactly the parameter range which we use in figure 3, although we do not work in an extremal feedback limit. There we have chosen a rather high temperature $T_\alpha = 10\epsilon$. In the parametrization of the spectral densities in equation (8), we use $\epsilon_{\mathrm{L}} = 5\epsilon$ and $\epsilon_{\mathrm{R}} = -1\epsilon$.

Furthermore, we can infer from equation (20) that a large bias V results in a large time-averaged power $\overline{P}$. Although this has a detrimental effect on the averaged matter current $\overline{I}_{\mathrm{m}}$, the overall effect is indeed a large power as we can see in figure 3(a).

5. Discussion and conclusions

We have harnessed a DCG approach in order to conveniently describe the dynamics of the SET under the action of the Maxwell demon. We have implemented the demon by a piecewise-constant feedback scheme, where the occupation of the quantum dot is projectively measured with frequency $1/\tau$. The accuracy of the DCG has been tested by benchmarking it with the exact solution in the absence of feedback. For vanishing feedback times τ, which corresponds to a continuous observation of the system by the demon, we resembled the quantum-Zeno effect by which the current between the reservoirs is blocked. Moreover, we found that the power and efficiency are optimized for an intermediate feedback time τ outside of the quantum-Zeno regime. The performance of the system is also better for a large bias and higher temperatures. With the DCG method we could thus show that there is an intermediate regime between a genuine quantum effect and a classical rate equation dynamics to optimize the performance of a quantum device under dissipative conditions. This seems thus reminiscent to the interplay of quantum and dissipative effects in other transport scenarios [60–63].

Furthermore, we have discovered a novel aspect appearing in the quantum treatment of Maxwell's demon. Due to the projective measurement of the system, there is a parameter regime where the total system energy *decreases*. It is the regime where it is most profitable to run the setup. However, whether or not this work can be stored or harnessed to run a third task lies outside the scope of our methods. To approach this question a microscopic implementation of the measurement apparatus would be necessary in contrast to the bare effective description of the projective measurement applied here. A possible and experimentally realistic way would be to describe the measurement process by an adjacent quantum-point contact [64–66] or an autonomous feedback setup as investigated in [8, 57, 67].

Acknowledgments

Financial support by the DFG (SFB 910, GRK 1558, SCHA 1646/3-1, BR 1928/9-1), the WE-Heraeus foundation (WEH 640) and the Natural Science Foundation of China (under Grant No.:U1530401) is gratefully acknowledged. We thank Philipp Strasberg and Javier Cerrillo for constructive discussions.

Appendix. Heat entering the reservoirs

In figure A1, we depict the amounts of heat transported to the single reservoirs $\alpha = \mathrm{R},\ \mathrm{L}$. Overall, the respective heat amounts differ strongly from the total heat Q depicted in figure 3(c). In the region, where the transported amount of heat is overall negative $Q < 0$, we find that the heat amounts into the reservoirs Q_α is rather small or even negative. If the overall amount of heat is positive $Q > 0$, then only either reservoir experiences a strong increase of heat. For $V < 0$, the heat in the right reservoir strongly increases and for $V < 0$, the heat in the left reservoir strongly increases.

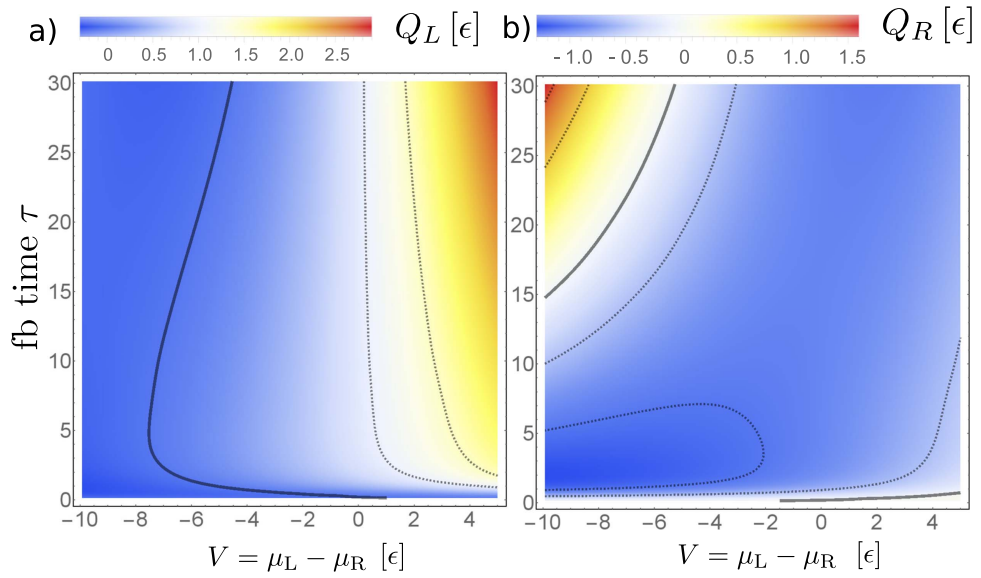

Figure A1. (a) Amount of heat entering the left reservoir within one period. (b) Amount of heat entering the right reservoir within one feedback period. The parameters are as in figure 3.

ORCID iDs

G Engelhardt https://orcid.org/0000-0002-0791-3617
G Schaller https://orcid.org/0000-0003-0062-9944

References

[1] Maruyama K, Nori F and Vedral V 2009 Colloquium: the physics of Maxwell's demon and information *Rev. Mod. Phys.* **81** 1–23
[2] Leff H S and Rex A F 2014 *Maxwell's Demon: Entropy, Information, Computing* (Princeton, NJ: Princeton University Press)
[3] Szilard L 1929 Über die Entropieverminderung in einem thermodynamischen System bei Eingriffen intelligenter Wesen *Z. Phys.* A **53** 840–56
[4] Brillouin L 1951 Maxwell's demon cannot operate: information and entropy: I *J. Appl. Phys.* **22** 334–7
[5] Bennett C H 1982 The thermodynamics of computation—a review *Int. J. Theor. Phys.* **21** 905–40
[6] Landauer R 1961 Irreversibility and heat generation in the computing process *IBM J. Res. Dev.* **5** 183–91
[7] Chida K, Desai S, Nishiguchi K and Fujiwara A 2017 Power generator driven by Maxwell's demon *Nat. Commun.* **8** 15310
[8] Strasberg P, Schaller G, Brandes T and Esposito M 2013 Thermodynamics of a physical model implementing a Maxwell demon *Phys. Rev. Lett.* **110** 040601
[9] Strasberg P, Schaller G, Brandes T and Jarzynski C 2014 Second laws for an information driven current through a spin valve *Phys. Rev.* E **90** 062107
[10] Kutvonen A, Koski J and Ala-Nissilä T 2016 Thermodynamics and efficiency of an autonomous on-chip Maxwell's demon *Sci. Rep.* **6** 21126
[11] Rosselló G, López R and Platero G 2017 Chiral Maxwell demon in a quantum Hall system with a localized impurity *Phys. Rev.* B **96** 075305
[12] Strasberg P, Schaller G, Brandes T and Esposito M 2017 Quantum and information thermodynamics: a unifying framework based on repeated interactions *Phys. Rev.* X **7** 021003
[13] Schaller G, Emary C, Kiesslich G and Brandes T 2011 Probing the power of an electronic Maxwell's demon: single-electron transistor monitored by a quantum point contact *Phys. Rev.* B **84** 085418
[14] Averin D V, Möttönen M and Pekola J P 2011 Maxwell's demon based on a single-electron pump *Phys. Rev.* B **84** 245448
[15] Kish L B and Granqvist C G 2012 Electrical Maxwell demon and Szilard engine utilizing Johnson noise, measurement, logic and control *PLoS One* **7** e46800
[16] Esposito M and Schaller G 2012 Stochastic thermodynamics for Maxwell demon feedbacks *Europhys. Lett.* **99** 30003
[17] Bergli J, Galperin Y M and Kopnin N B 2013 Information flow and optimal protocol for a Maxwell-demon single-electron pump *Phys. Rev.* E **88** 062139
[18] Sothmann B, Sánchez R and Jordan A N 2015 Thermoelectric energy harvesting with quantum dots *Nanotechnology* **26** 032001
[19] Sánchez R and Büttiker M 2011 Optimal energy quanta to current conversion *Phys. Rev.* B **83** 085428
[20] Hartmann F, Pfeffer P, Höfling S, Kamp M and Worschech L 2015 Voltage fluctuation to current converter with Coulomb-coupled quantum dots *Phys. Rev. Lett.* **114** 146805
[21] Koski J V, Maisi V F, Pekola J P and Averin D V 2014 Experimental realization of a Szilard engine with a single electron *Proc. Natl Acad. Sci.* **111** 13786–9
[22] Strasberg P, Schaller G, Schmidt T L and Esposito M 2017 Fermionic reaction coordinates and their application to an autonomous Maxwell demon in the strong coupling regime arXiv:1711.08914
[23] Koski J V, Maisi V F, Sagawa T and Pekola J P 2014 Experimental observation of the role of mutual information in the nonequilibrium dynamics of a Maxwell demon *Phys. Rev. Lett.* **113** 030601

[24] Camati P A, Peterson J P S, Batalhão T B, Micadei K, Souza A M, Sarthour R S, Oliveira I S and Serra R M 2016 Experimental rectification of entropy production by Maxwell's demon in a quantum system *Phys. Rev. Lett.* **117** 240502
[25] Cai C Y, Dong H and Sun C P 2012 Multiparticle quantum Szilard engine with optimal cycles assisted by a Maxwell's demon *Phys. Rev.* E **85** 031114
[26] Dong H, Xu D Z, Cai C Y and Sun C P 2011 Quantum Maxwell's demon in thermodynamic cycles *Phys. Rev.* E **83** 061108
[27] Quan H T, Wang Y D, Liu Y X, Sun C P and Nori F 2006 Maxwell's demon assisted thermodynamic cycle in superconducting quantum circuits *Phys. Rev. Lett.* **97** 180402
[28] Schaller G and Brandes T 2008 Preservation of positivity by dynamical coarse graining *Phys. Rev.* A **78** 022106
[29] Schaller G 2014 *Open Quantum Systems Far from Equilibrium* vol 881 (Berlin: Springer)
[30] Lidar D A, Bihary Z and Whaley K B 2001 From completely positive maps to the quantum Markovian semigroup master equation *Chem. Phys.* **268** 35–53
[31] Majenz C, Albash T, Breuer H-P and Lidar D A 2013 Coarse graining can beat the rotating-wave approximation in quantum Markovian master equations *Phys. Rev.* A **88** 012103
[32] Schaller G, Zedler P and Brandes T 2009 Systematic perturbation theory for dynamical coarse-graining *Phys. Rev.* A **79** 032110
[33] Zedler P, Schaller G, Kießlich G, Emary C and Brandes T 2009 Weak-coupling approximations in non-Markovian transport *Phys. Rev.* B **80** 045309
[34] Rivas Á 2017 Refined weak-coupling limit: coherence, entanglement, and non-Markovianity *Phys. Rev.* A **95** 042104
[35] Schaller G, Kießlich G and Brandes T 2009 Transport statistics of interacting double dot systems: coherent and non-Markovian effects *Phys. Rev.* B **80** 245107
[36] Misra B and Sudarshan E C G 1977 The Zeno's paradox in quantum theory *J. Math. Phys.* **18** 756–63
[37] Itano W M, Heinzen D J, Bollinger J J and Wineland D J 1990 Quantum zeno effect *Phys. Rev.* A **41** 2295–300
[38] Fischer M C, Gutiérrez-Medina B and Raizen M G 2001 Observation of the quantum Zeno and anti-Zeno effects in an unstable system *Phys. Rev. Lett.* **87** 040402
[39] Gurvitz S A 1991 Josephson-type effect in resonant-tunneling heterostructures *Phys. Rev.* B **44** 11924–32
[40] Topp G E, Brandes T and Schaller G 2015 Steady-state thermodynamics of non-interacting transport beyond weak coupling *Europhys. Lett.* **110** 67003
[41] Engelhardt G, Schaller G and Brandes T 2016 Bosonic Josephson effect in the Fano–Anderson model *Phys. Rev.* A **94** 013608
[42] Kammerlander P and Anders J 2016 Coherence and measurement in quantum thermodynamics *Sci. Rep.* **6** 22174
[43] Brandner K, Bauer M, Schmid M T and Seifert U 2015 Coherence-enhanced efficiency of feedback-driven quantum engines *New J. Phys.* **17** 065006
[44] Elouard C, Herrera-Martí D A, Clusel M and Auffèves A 2017 The role of quantum measurement in stochastic thermodynamics *NPJ Quantum Inf.* **3** 9
[45] Elouard C, Herrera-Martí D, Huard B and Auffèves A 2017 Extracting work from quantum measurement in Maxwell's demon engines *Phys. Rev. Lett.* **118** 260603
[46] Wiseman H M and Milburn G J 2009 *Quantum Measurement and Control* (Cambridge: Cambridge University Press)
[47] Schaller G 2012 Fighting decoherence by feedback-controlled dissipation *Phys. Rev.* A **85** 062118
[48] Gurvitz S A 1998 Rate equations for quantum transport in multidot systems *Phys. Rev.* B **57** 6602–11
[49] Brandes T 2005 Coherent and collective quantum optical effects in mesoscopic systems *Phys. Rep.* **408** 315–474
[50] Contreras-Pulido L D, Bruderer M, Huelga S F and Plenio M B 2014 Dephasing-assisted transport in linear triple quantum dots *New J. Phys.* **16** 113061
[51] Schaller G, Cerrillo J, Engelhardt G and Strasberg P 2017 An electronic Maxwell demon in the coherent strong-coupling regime arXiv:1711.00706
[52] Deffner S 2013 Information-driven current in a quantum Maxwell demon *Phys. Rev.* E **88** 062128
[53] Bozkurt A M, Pekerten B and Adagideli I 2017 Work extraction and Landauer's principle in a quantum spin Hall device arXiv:1705.04985
[54] Esposito M, Lindenberg K and Van den Broeck C 2010 Entropy production as correlation between system and reservoir *New J. Phys.* **12** 013013
[55] Li S-W 2017 Production rate of the system-bath mutual information *Phys. Rev.* E **96** 012139
[56] Pucci L, Esposito M and Peliti L 2013 Entropy production in quantum Brownian motion *J. Stat. Mech.* P04005
[57] Horowitz J M and Esposito M 2014 Thermodynamics with continuous information flow *Phys. Rev.* X **4** 031015
[58] Sagawa T and Ueda M 2008 Second law of thermodynamics with discrete quantum feedback control *Phys. Rev. Lett.* **100** 080403
[59] Sagawa T and Ueda M 2012 Nonequilibrium thermodynamics of feedback control *Phys. Rev.* E **85** 021104
[60] Xu D, Wang C, Zhao Y and Cao J 2016 Polaron effects on the performance of light-harvesting systems: a quantum heat engine perspective *New J. Phys.* **18** 023003
[61] Xu D and Cao J 2016 Non-canonical distribution and non-equilibrium transport beyond weak system-bath coupling regime: a polaron transformation approach *Front. Phys.* **11** 110308
[62] Liu J, Xu H, Li B and Wu C 2017 Energy transfer in the nonequilibrium spin-boson model: from weak to strong coupling *Phys. Rev.* E **96** 012135
[63] Wu J, Silbey R J and Cao J 2013 Generic mechanism of optimal energy transfer efficiency: a scaling theory of the mean first-passage time in exciton systems *Phys. Rev. Lett.* **110** 200402
[64] Flindt C, Fricke C, Hohls F, Novotný T, Netočny` K, Brandes T and Haug R J 2009 Universal oscillations in counting statistics *Proc. Natl Acad. Sci. USA* **106** 10116–9
[65] Wagner T, Strasberg P, Bayer J C, Rugeramigabo E P, Brandes T and Haug R J 2017 Strong suppression of shot noise in a feedback-controlled single-electron transistor *Nat. Nanotechnol.* **12** 218–22
[66] Fujisawa T, Hayashi T, Tomita R and Hirayama Y 2006 Bidirectional counting of single electrons *Science* **312** 1634–6
[67] Koski J V, Kutvonen A, Khaymovich I M, Ala-Nissila T and Pekola J P 2015 On-chip Maxwell's demon as an information-powered refrigerator *Phys. Rev. Lett.* **115** 260602